Journal of Materials Chemistry B

ROYAL SOCIETY OF CHEMISTRY

PAPER

View Article Online
View Journal | View Issue

Cite this: J. Mater. Chem. B, 2023, 11, 3635

Theranostic inorganic–organic hybrid nanoparticles with a cocktail of chemotherapeutic and cytostatic drugs†

Mikhail Khorenko,[a] Juliana Pfeifer,[b] Joanna Napp,[de] Anna Meschkov,[bc] Frauke Alves,*[de] Ute Schepers*[bc] and Claus Feldmann*[a]

Theranostic inorganic–organic hybrid nanoparticles (IOH-NPs) with a cocktail of chemotherapeutic and cytostatic drugs and a composition $Gd_2^{3+}[(PMX)_{0.5}(EMP)_{0.5}]_3^{2-}$, $[Gd(OH)]^{2+}[(PMX)_{0.74}(AlPCS_4)_{0.13}]^{2-}$, or $[Gd(OH)]^{2+}[(PMX)_{0.70}(TPPS_4)_{0.15}]^{2-}$ (PMX: pemetrexed, EMP: estramustine phosphate, $AlPCS_4$: aluminum(III) chlorido phthalocyanine tetrasulfonate, $TPPS_4$: tetraphenylporphine sulfonate) are presented for the first time. These IOH-NPs are prepared in water (40–60 nm in size) and have a non-complex composition with outstanding drug loading (71–82% of total nanoparticle mass) of at least two chemotherapeutic or a mixture of cytostatic and photosensitizing agents. All IOH-NPs show red to deep-red emission (650–800 nm) to enable optical imaging. The superior performance of the IOH-NPs with a chemotherapeutic/cytostatic cocktail is validated based on cell-viability assays and angiogenesis studies with human umbilical vein endothelial cells (HUVEC). The synergistic anti-cancer effect of the IOH-NPs with a chemotherapeutic cocktail is shown in a murine breast-cancer cell line (pH8N8) and a human pancreatic cancer cell line (AsPC1), whereas the synergistic cytotoxic and phototoxic efficacy is verified in response to illumination of HeLa-GFP cancer cells, MTT assays with human colon cancer cells (HCT116), and normal human dermal fibroblasts (NHDF). HepG2 spheroids as 3D cell cultures prove the effective uptake of the IOH-NPs with high uniform distribution and the release of the chemotherapeutic drugs with the strong synergistic effect of the cocktail of drugs.

Received 4th February 2023,
Accepted 17th March 2023

DOI: 10.1039/d3tb00226h

rsc.li/materials-b

1. Introduction

Nanocarriers loaded with chemotherapeutics belong to the first of still few nanocarrier formulations that received clinical approval.[1] First examples in oncology are non-PEGylated liposomal doxorubicin (Myocet®) or PEGylated liposomal doxorubicin (Caelyx®, Doxil®).[2] Such nanoparticulate formulations can have several advantages over the freely dissolved chemotherapeutics such as less side effects, the use of higher doses over shorter periods of time, an increased drug accumulation in tumours and/or a reduced off-target uptake in comparison to the freely dissolved chemotherapeutic agent.[1,2a] Moreover, nanocarriers allow straightforward incorporation of imaging probes for concurrent assessment of tumour-drug delivery and targeting.[3] Besides a few clinically approved nanotherapeutics, several nanocarrier-based concepts have been suggested for the transport of chemotherapeutics from the viewpoint of materials science.[1,2,4] Typically, the chemotherapeutic agent is encapsulated in a certain matrix such as organic polymers (*e.g.* polyethylenglycol/PEG) or biopolymers (*e.g.*, polysaccharides, polypeptides),[5] liposomes or micelles,[6] or inorganic matrices such as silica, iron oxides, and metal phosphates.[7] By far the largest number of these nanocarrier concepts is limited to *in vitro* experiments and was not assessed *in vivo* due to unexpected side effects, low activity, low biocompatibility, or unknown reasons. Many nanocarrier systems yet suffer from weaknesses such as inadequate drug loading (often <20% of total nanocarrier mass), high material complexity, uncontrolled drug leakage, limited cell uptake, damage of cell membranes, unexpected toxicity and/or hypersensitivity. All in all, further improvement and exploration of alternative, more robust delivery systems with high drug loadings are indispensable.

[a] Institute of Inorganic Chemistry, Karlsruhe Institute of Technology (KIT), Engesserstraße 15, 76131 Karlsruhe, Germany. E-mail: claus.feldmann@kit.edu
[b] Institute of Functional Interfaces, Karlsruhe Institute of Technology (KIT), Hermann-von-Helmholtz-Platz 1, 76344 Eggenstein-Leopoldshafen, Germany. E-mail: ute.schepers@kit.edu
[c] Institute of Organic Chemistry, Karlsruhe Institute of Technology (KIT), Fritz-Haber Weg 6, 76131 Karlsruhe, Germany
[d] University Medical Center Goettingen (UMG), Institute for Diagnostic and Interventional Radiology, Robert Koch Str. 40, 37075 Goettingen, Germany. E-mail: falves@gwdg.de
[e] Max Planck Institute for Multidisciplinary Sciences, Translational Molecular Imaging, City campus, Hermann-Rein-Strasse 3, 37075 Göttingen, Germany

† Electronic supplementary information (ESI) available: Further details regarding analytical equipment, chemical synthesis, characterization of IOH-NPs, and additional information regarding cell assays and spheroid studies. See DOI: https://doi.org/10.1039/d3tb00226h

In addition to the most often studied delivery of a single chemotherapeutic agent, a simultaneous release of two chemotherapeutics with high concentration at the same time and the same site of action would be desirable.[8] Specifically, this holds for tumour treatment in order to reduce the therapeutic dose of an individual drug, to enhance anticancer efficacy due to synergistic or additive effects, and/or to minimize the risk of multi-drug resistance. Such nanocarriers with a combination of chemotherapeutic and/or cytotoxic agents were barely addressed although such adjunctive approaches are most relevant in the clinics.[4–7] In this regard, the design of smart nanoplatforms for combinational therapy has the potential to be the next-generation cancer-treatment regime. Examples of the most common chemotherapeutic agents that are used alone or in combination are doxorubicin (DOX), paclitaxel (PTX), camptothecin (CPT), methotrexate (MTX), and curcumin.[9]

Aiming at nanocarriers with a high-load chemotherapeutic or cytotoxic cocktail, we here suggest inorganic–organic hybrid nanoparticles (IOH-NPs). IOH-NPs have a saline composition with an inorganic cation and a functional organic anion.[10] They are prepared in water and have an uncomplex composition and structure such as $[Gd(OH)]^{2+}[(\text{active agent A})(\text{active agent B})]^{2-}$ with an extremely high load of active agents (60–80% of total nanoparticle mass). Here, we exemplary combine the chemotherapeutic drugs pemetrexed (PMX) and estramustine phosphate (EMP) as well as the chemotherapeutic PMX with the photosensitizing agents aluminum(III) chlorido phthalocyanine tetrasulfonate ($AlPCS_4$) or tetraphenylporphine sulfonate ($TPPS_4$). IOH-NPs with such a chemotherapeutic or cytostatic cocktail are presented for the first time. They are evaluated in different tumour-cell assays and in 3D tumour spheroids.

2. Experimental section

$Gd_2^{3+}[PMX]_3^{2-}$ IOH-NPs (PMX, pemetrexed, $C_{20}H_{21}N_5O_6$) were prepared by injecting 0.5 mL of an aqueous solution of $GdCl_3 \times 6H_2O$ (18.6 mg, 0.05 mmol, 99%, Sigma, Germany) into 50 mL of a vigorously stirred solution of $Na_2(PMX) \times 7H_2O$ (35.4 mg, 0.06 mmol, ≥98%, VWR, Germany). After 30 min of intense stirring, the IOH-NPs were separated by centrifugation (15 min at 25 000 rpm) and redispersed in H_2O (10 mL). To remove all the remaining starting materials and salts, the colourless solid was thrice redispersed/centrifuged in/from water for purification. Finally, the IOH-NPs were redispersed in sterilized water.

$[Gd(OH)]^{2+}[EMP]^{2-}$ IOH-NPs (EMP, estramustine phosphate, $C_{23}H_{32}Cl_2NO_6P$) were prepared by injecting 0.5 mL of an aqueous solution of $GdCl_3 \times 6H_2O$ (18.6 mg, 0.05 mmol) into 50 mL of a vigorously stirred solution of $Na_2(EMP)$ (45.4 mg, 0.08 mmol, >98%, MedChemTronica, Sweden). After 30 min of intense stirring, the IOH-NPs were separated *via* centrifugation. Separation and purification were performed similarly to $Gd_2^{3+}[PMX]_3^{2-}$ IOH-NPs.

$Gd_2^{3+}[(PMX)_{0.5}(EMP)_{0.5}]_3^{2-}$ IOH-NPs were prepared by injecting 0.5 mL of an aqueous solution of $GdCl_3 \times 6H_2O$ (18.6 mg, 0.05 mmol) into 50 mL of a vigorously stirred solution of $Na_2(PMX) \times 7H_2O$ (17.7 mg, 0.03 mmol) and $Na_2(EMP)$ (21.3 mg, 0.04 mmol). After 30 min of intense stirring, the IOH-NPs were separated *via* centrifugation. Separation and purification were performed similarly to the $Gd_2^{3+}[PMX]_3^{2-}$ IOH-NPs.

Fluorescence labelling

Fluorescence labelling of $Gd_2^{3+}[PMX]_3^{2-}$, $[Gd(OH)]^{2+}[EMP]^{2-}$, and $Gd_2^{3+}[(PMX)_{0.50}(EMP)_{0.50}]_3^{2-}$ IOH-NPs was performed by addition of the deep-red emitting dyes indocyanine green (ICG) or dye-modified nucleoside triphosphate DY-647-dUTP. To this concern, the syntheses were performed as described before but with ICG or DUT in addition. For ICG-labelling, Na(ICG) (3.9 mg, 0.005 mmol, $C_{43}H_{47}N_2NaO_6S_2$, abcr, Germany) was added to the solutions of the anionic drugs before injecting the $GdCl_3 \times 6H_2O$ solution resulting in compositions $Gd_2^{3+}[(PMX)_{0.96}(ICG)_{0.08}]_3^{2-}$, $[Gd(OH)]^{2+}[(EMP)_{0.94}(ICG)_{0.12}]^{2-}$, $Gd_2^{3+}[(PMX)_{0.50}(EMP)_{0.47}(ICG)_{0.06}]_3^{2-}$. For DUT-labelling, DUT (1.1 mg, DY-647-dUTP, Dyomics, Germany) was added to the solutions of the anionic drugs before injecting the $GdCl_3 \times 6H_2O$ solution resulting in compositions $Gd_2^{3+}[(PMX)_{0.99}(DUT)_{0.01}]_3^{2-}$, $[Gd(OH)]^{2+}[(EMP)_{0.99}(DUT)_{0.01}]^{2-}$, and $Gd_2^{3+}[(PMX)_{0.50}(EMP)_{0.49}(DUT)_{0.02}]_3^{2-}$.

$[Gd(OH)]^{2+}[(PMX)_{0.74}(AlPCS_4)_{0.13}]^{2-}$ IOH-NPs ($AlPCS_4$: aluminum(III) chlorido phthalocyanine tetrasulfonate, $C_{32}H_{16}AlClN_8O_{12}S_4$) were prepared by injecting 0.5 mL of an aqueous solution of $GdCl_3 \times 6H_2O$ (29.8 mg, 0.08 mmol, 99%, Sigma, Germany) into 50 mL of a vigorously stirred solution of $Na_2(PMX) \times 7H_2O$ (44.1 mg, 0.074 mmol) and $H_4(AlPCS_4)$ (39.3 mg, 0.04 mmol, Frontier Scientific, USA), which had been previously adjusted to a pH of 7 upon addition of 0.1 M NaOH. After 30 min of intense stirring, the IOH-NPs were separated *via* centrifugation. Separation and purification were performed similarly to $Gd_2^{3+}[PMX]_3^{2-}$.

$[Gd(OH)]^{2+}[(PMX)_{0.70}(TPPS_4)_{0.15}]^{2-}$ IOH-NPs ($TPPS_4$: tetraphenylporphine sulfonate, $C_{44}H_{26}N_4O_{12}S_4$) were prepared by injecting 0.5 mL of an aqueous solution of $GdCl_3 \times 6H_2O$ (29.8 mg, 0.08 mmol, 99%, Sigma, Germany) into 50 mL of a vigorously stirred solution of $Na_2(PMX) \times 7H_2O$ (41.8 mg, 0.07 mmol) and $H_4(TPPS_4) \times 10H_2O$ (37.2 mg, 0.03 mmol, Frontier Scientific, USA), which had been previously adjusted to a pH of 7 upon addition of 0.1 M NaOH. After 30 min of intense stirring, the IOH-NPs were separated *via* centrifugation. Separation and purification were performed similarly to the $Gd_2^{3+}[PMX]_3^{2-}$ IOH-NPs.

Further data regarding analytical equipment, material characterization, *in vitro* assays and 3D tumour spheroids are detailed in the ESI.†

3. Results and discussion

3.1 Material concept and nanoparticle synthesis

Aiming at an aqueous synthesis of nanocarriers for drug delivery with a simple material composition and structure as well as a high drug load (>60% of total nanoparticle mass), we have developed the concept of inorganic–organic hybrid nanoparticles (IOH-NPs).[10] IOH-NPs have a saline composition with

an inorganic cation and a drug anion, which is functionalized by phosphate, sulfonate, or carboxylate groups. In combination with a suitable cation, the drug anion forms an insoluble saline compound in water. Specific examples, for instance, are $[ZrO]^{2+}[FdUMP]^{2-}$, $[ZrO]^{2+}[BMP]^{2-}$ or $[ZrO]^{2+}[CLP]^{2-}$, containing the chemotherapeutic agent 5′-fluoro-2′-deoxyuridine-5′-monophosphate (FdUMP), the glucocorticoid betamethasone phosphate (BMP), or the antibiotic clindamycin phosphate (CLP) as drug anions.[10b,11] Besides the aqueous synthesis and the new nanocarrier concept for drug delivery, the high drug load is a characteristic feature of these IOH-NPs. Thus, $[ZrO]^{2+}[FdUMP]^{2-}$, $[ZrO]^{2+}[BMP]^{2-}$, and $[ZrO]^{2+}[CLP]^{2-}$ have drug loads of 75% of FdUMP, 81% of BMP, and 82% of CLP per nanoparticle.

In principle, the IOH-NP concept could also allow the simultaneous combination of different types of active agents in a single nanoparticle, which is aimed here for the first time. Such a combination of active agents seems most interesting for tumour therapy and may help to reduce the risks of resistance and metastasis. As a first proof-of-concept, we have combined the two chemotherapeutic drugs pemetrexed (PMX) and estramustine phosphate (EMP) in $Gd_2^{3+}[(PMX)_{0.5}(EMP)_{0.5}]_3^{2-}$ IOH-NPs (Fig. 1(a)). PMX and EMP are clinically approved and used for the therapy of, *e.g.*, breast, lung, and prostate cancer. Both PMX and EMP are also known to cause severe side effects (*e.g.*, nausea, vomiting, gynecomastia, feminization, demasculinization, sexual dysfunction, blood clots, and cardiovascular complications).[12] In addition, the chemotherapeutic PMX is combined with the photosensitizing agents aluminum(III) chlorido phthalocyanine tetrasulfonate ($AlPCS_4$) or tetraphenylporphine sulfonate ($TPPS_4$), resulting in $[Gd(OH)]^{2+}[(PMX)_{0.74}(AlPCS_4)_{0.13}]^{2-}$ and $[Gd(OH)]^{2+}[(PMX)_{0.70}(TPPS_4)_{0.15}]^{2-}$ IOH-NPs (Fig. 1(b)). Such phthalocyanines and porphyrins are clinically approved and used for photodynamic therapy (PDT).[13] Based on the IOH-NP concept, we here aim at IOH-NPs with a chemotherapeutic and cytotoxic cocktail for the first time.

In principle, the synthesis is straightforward and performed by water-based precipitation at room temperature (Fig. 1). Accordingly, a concentrated aqueous solution of $GdCl_3 \times 6H_2O$ was injected with vigorous stirring into an aqueous solution of the respective active agent (*i.e.*, $Na_2(EMP)$, $Na_2(PMX)$, $H_4(AlPCS_4)$, $H_4(TPPS_4)$). Following the LaMer–Dinegar model of particle nucleation and particle growth,[14] a high supersaturation was induced upon injection and resulted in rapid particle nucleation, favouring the formation of small-sized nanoparticles. The as-prepared $Gd_2^{3+}[PMX]_3^{2-}$, $[Gd(OH)]^{2+}[EMP]^{2-}$, $Gd_2^{3+}[(PMX)_{0.5}(EMP)_{0.5}]_3^{2-}$, $[Gd(OH)]^{2+}[(PMX)_{0.74}(AlPCS_4)_{0.13}]^{2-}$ and $[Gd(OH)]^{2+}[(PMX)_{0.70}(TPPS_4)_{0.15}]^{2-}$ IOH-NPs were purified by repeated centrifugation/redispersion in/from water to remove remaining starting materials and salts. Thereafter, the IOH-NPs were dried to powder samples or redispersed to obtain colloidally stable suspensions in water (Fig. 1).

3.2 Nanoparticle characterization

The novel $Gd_2^{3+}[PMX]_3^{2-}$, $[Gd(OH)]^{2+}[EMP]^{2-}$, $Gd_2^{3+}[(PMX)_{0.5}(EMP)_{0.5}]_3^{2-}$, $[Gd(OH)]^{2+}[(PMX)_{0.74}(AlPCS_4)_{0.13}]^{2-}$ and $[Gd(OH)]^{2+}[(PMX)_{0.70}(TPPS_4)_{0.15}]^{2-}$ IOH-NPs were characterized in regard of particle size, size distribution and colloidal stability, chemical composition and fluorescence labelling. First of all, particle size and colloidal properties were addressed. According to dynamic light scattering (DLS), aqueous suspensions of the as-prepared IOH-NPs exhibit mean hydrodynamic diameters of 60 to 100 nm (Table 1, and Fig. 2(a), (d); ESI,† Fig. S1–S3, S7, S8). Scanning electron microscopy (SEM) confirms the presence of spherical particles with mean diameters of 40 to 60 nm (Table 1 and Fig. 2(a), (c), (d), (f); ESI,† Fig. S1–S3, S7, S8). The latter values were calculated by a statistical evaluation of >100 particles on SEM

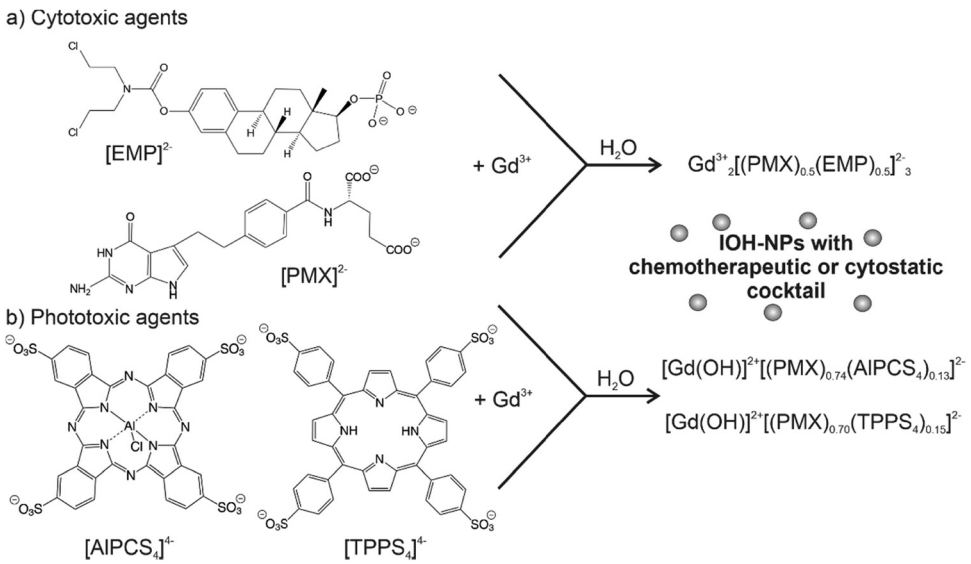

Fig. 1 Scheme illustrating the aqueous synthesis of IOH-NPs with a cocktail of chemotherapeutic and cytostatic drugs: (a) $Gd_2^{3+}[(PMX)_{0.5}(EMP)_{0.5}]_3^{2-}$ with pemetrexed (PMX) and estramustine phosphate (EMP); (b) $[Gd(OH)]^{2+}[(PMX)_{0.74}(AlPCS_4)_{0.13}]^{2-}$ and $[Gd(OH)]^{2+}[(PMX)_{0.70}(TPPS_4)_{0.15}]^{2-}$ with pemetrexed (PMX), aluminum(III) chlorido phthalocyanine tetrasulfonate ($AlPCS_4$) and tetraphenylporphine sulfonate ($TPPS_4$).

Table 1 Particle size and zeta potential of the as-prepared IOH-NPs

	Particle size/nm (according to DLS)	Particle size/nm (according to SEM)	Zeta potential/mV (at pH 7.0)
$Gd_2^{3+}[(PMX)_{0.5}(EMP)_{0.5}]_3^{2-}$	82 ± 17	35 ± 2	−34
$Gd_2^{3+}[PMX]_3^{2-}$	97 ± 18	59 ± 5	−20
$[Gd(OH)]^{2+}[EMP]^{2-}$	60 ± 16	26 ± 2	−12
$[Gd(OH)]^{2+}[(PMX)_{0.74}(AlPCS_4)_{0.13}]^{2-}$	98 ± 21	55 ± 3	−33
$Gd_4^{3+}[AlPCS_4]_3^{4-}$ [a]	Not measured	47 ± 4	−26
$[Gd(OH)]^{2+}[(PMX)_{0.70}(TPPS_4)_{0.15}]^{2-}$	59 ± 27	42 ± 3	−20
$La_4^{3+}[TPPS_4]_3^{4-}$ [a]	Not measured	68 ± 8	−34

[a] The pseudo-binary compounds $Gd_4^{3+}[AlPCS_4]_3^{4-}$ and $La_4^{3+}[TPPS_4]_3^{4-}$ were characterized and discussed elsewhere.

images. The larger particle diameter from DLS reflects the hydrodynamic diameter and the presence of a rigid layer of water molecules adsorbed on the particle surface. The IOH-NPs form colloidally stable suspensions without the need for any additional surface-active agents for size control and/or colloidal stabilization, which further facilitate the synthesis and also enable to keep a simple structure and composition of the nanocarriers. The good colloidal stability of the IOH-NPs can be ascribed to the intrinsic charge stabilization as indicated by zeta-potential measurements (Table 1 and Fig. 2(b), (e); ESI,† Fig. S1–S3, S7, S8). Thus, negative charging of −15 to −35 mV is observed in water in the physiologically relevant pH range of 6.5–7.5. Typically, the as-prepared IOH-NP suspensions do not show any sedimentation over a period of 3–4 weeks.

To prove the chemical composition of the IOH-NPs, different analytical methods were involved. X-ray diffraction (XRD) indicated the IOH-NPs to be non-crystalline (Fig. S4, ESI†), which is not a surprise when taking the large volume of active anions and the low temperature of synthesis into account. In fact, such amorphous drug nanocarriers can be ideal in regard to their dissolution kinetics,[16] being slow enough to achieve maintenance of high tumour concentrations, whilst rapid enough to avoid side effects due to particle accumulation. Fourier-transform infrared (FT-IR) spectroscopy evidences the presence of the respective active anion (ESI,† Fig. S1–S3, S7 and S8). Thus, the characteristic vibrations of the drug anion are observed and well in agreement with the starting material as a reference. Energy dispersive X-ray spectroscopy (EDXS) confirms the presence of gadolinium, phosphorus and sulphur in the IOH-NPs. Finally, the chemical composition of the IOH-NPs was quantified by total organics combustion *via* thermogravimetry (TG) and elemental analysis (EA) (Table 2; ESI,† Tables S1, S2 and Fig. S1–S3, S5, S7–S9). Here, the calculated values are in agreement with the experimental observation and confirm the cation-to-anion ratio as well as the overall composition of the IOH-NPs.

To enable IOH-NPs with chemotherapeutic cocktail for fluorescence-based monitoring, they were labelled with indocyanine green (ICG)[17] or Dyomics DY-647-dUTP (DUT) as a fluorescent dye (ESI,† Fig. S6). Both show deep-red emission with absorption at 600–800 nm (ICG) and 500–700 nm (DUT) as

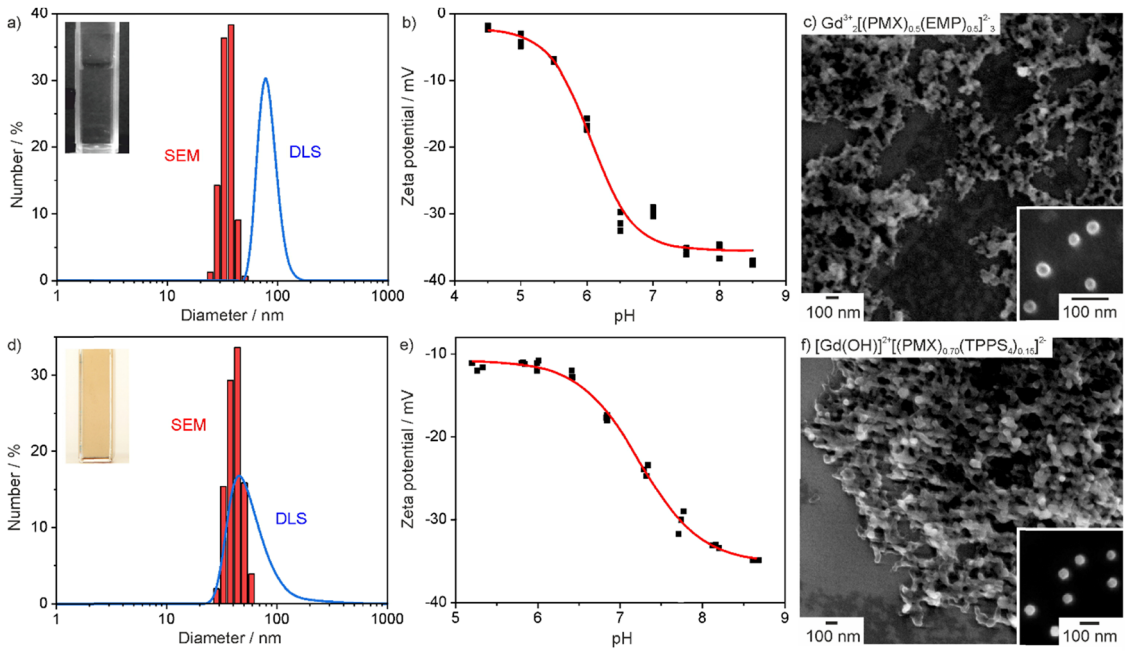

Fig. 2 Particle characterization of $Gd_2^{3+}[(PMX)_{0.5}(EMP)_{0.5}]_3^{2-}$ (a)–(c) and $[Gd(OH)]^{2+}[(PMX)_{0.70}(TPPS_4)_{0.15}]^{2-}$ (d)–(f) IOH-NPs: (a + d) Particle size distribution according to DLS and SEM, (b + e) Zeta potential of aqueous suspensions, (c + f) SEM images at different levels of magnification (for all further IOH-NPs see ESI,† Fig. S1–S3, S7, S8).

Table 2 Chemical composition of the as-prepared IOH-NPs

	Total organic content/% (according to TG)	Elemental analysis/%				Drug load/%
		C	H	N	S	
$Gd_2^{3+}[(PMX)_{0.5}(EMP)_{0.5}]_3^{2-}$	71.2	43.1	3.7	7.1	0.0	78.7
Calculated	*74.9*	*44.8*	*4.3*	*7.3*	*0*	*81.8*
$Gd_2^{3+}[PMX]_3^{2-}$	77.1	44.2	4.0	13.1	0.0	78.3
Calculated	*77.2*	*45.3*	*3.6*	*13.2*	*0*	*80.2*
$[Gd(OH)]^{2+}[EMP]^{2-}$	63.2	38.6	3.8	2.1	0.0	72.5
Calculated	*63.6*	*39.9*	*4.5*	*2.0*	*0*	*74.8*
$[Gd(OH)]^{2+}[(PMX)_{0.74}(AlPCS_4)_{0.13}]^{2-}$	70.4	37.7	3.5	10.9	2.8	71.2
Calculated	*68.9*	*37.7*	*2.8*	*11.0*	*2.8*	*71.3*
$Gd_4^{3+}[AlPCS_4]_3^{4-}$ [15 a]	79	36	3	13	8	81.2
Calculated	*78*	*35*	*1*	*10*	*11*	*81.0*
$[Gd(OH)]^{2+}[(PMX)_{0.70}(TPPS_4)_{0.15}]^{2-}$	73.5	41.0	3.7	9.6	3.1	72.6
Calculated	*70.4*	*40.5*	*3.0*	*9.4*	*3.2*	*71,5*
$La_4^{3+}[TPPS_4]_3^{4-}$ [15 a]	76	46	3	5	10	78.9
Calculated	*76*	*47*	*2*	*5*	*11*	*83.1*

[a] The pseudo-binary compounds $Gd_4^{3+}[AlPCS_4]_3^{4-}$ and $La_4^{3+}[TPPS_4]_3^{4-}$ were characterized and discussed elsewhere.

well as emission at 750–850 nm (ICG, λ_{max} = 810 nm) 630–780 nm (DUT, λ_{max} = 675 nm). Due to their intense emission, they are required only in very small portions (ICG: 5 mol%, DUT: 1 mol%). The cyto-/phototoxic IOH-NPs $[Gd(OH)]^{2+}[(PMX)_{0.74}(AlPCS_4)_{0.13}]^{2-}$ and $[Gd(OH)]^{2+}[(PMX)_{0.70}(TPPS_4)_{0.15}]^{2-}$ do not need any additional fluorescence labelling since $AlPCS_4$ and $TPPS_4$ show fluorescence themselves with strong absorption at 550–720 nm ($AlPCS_4$) and 380–600 nm ($TPPS_4$) as well as deep-red emission at 650–770 nm ($AlPCS_4$, λ_{max} = 686 nm) and 540–700 nm ($TPPS_4$, λ_{max} = 585 nm) (ESI,† Fig. S10).

3.3 *In vitro* studies with IOH-NPs and chemotherapeutic cocktail

Prior to the examination of the activity of IOH-NPs with a chemotherapeutic cocktail, first of all, the uptake by tumour cells and the detectability of the DUT-related emission were studied. To this concern, $Gd_2^{3+}[(PMX)_{0.50}(EMP)_{0.49}(DUT)_{0.01}]_3^{2-}$ IOH-NPs were selected. Since they contain both drugs, they can be also considered to be representative also for the single-drug IOH-NPs. The uptake of the photosensitizing IOH-NPs $Gd_4^{3+}[AlPCS_4]_3^{4-}$ and $La_4^{3+}[TPPS_4]_3^{4-}$ was already studied elsewhere.[15] $Gd_2^{3+}[(PMX)_{0.50}(EMP)_{0.49}(DUT)_{0.01}]_3^{2-}$ IOH-NPs (50 μL of IOH-NP suspension per 1 mL of cell culture medium) were incubated with 5×10^5 adhearent murine breast-cancer cells (pH8N8 cells)[18] and human pancreatic cancer cells (AsPC1 cells) over 48 h. Thereafter, the IOH-NP uptake was examined by recording the DUT-derived fluorescence *via* confocal microscopy (Fig. 3 and ESI,† Fig. S11).[19] After incubation, both pH8N8 breast-cancer cells and AsPC1 pancreatic-cancer cells have efficiently taken up the $Gd_2^{3+}[(PMX)_{0.50}(EMP)_{0.49}(DUT)_{0.01}]_3^{2-}$ IOH-NPs. Some uptake was already visible within the first 2–5 h of incubation, and the

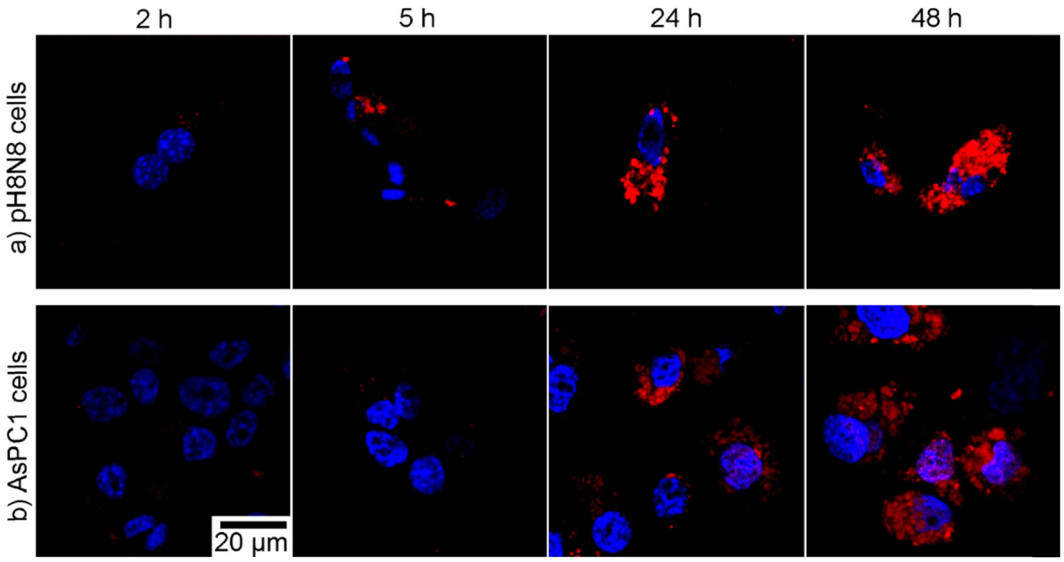

Fig. 3 Time-dependent uptake of DUT-labelled $Gd_2^{3+}[(PMX)_{0.50}(EMP)_{0.49}(DUT)_{0.01}]_3^{2-}$ IOH-NPs by (a) pH8N8 cells and (b) AsPC1 cells (5×10^5 cells per well) incubated over 2–48 h with 50 μL mL^{-1} of IOH-NPs. DAPI was excited with a 405 nm laser and the emission collected at 415–500 nm (blue). DUT was excited using a 633 nm laser and the emission collected at 645–780 nm (red), (identical scale bar for all images; see ESI,† Fig. S11 for overview images).

amount of the IOH-NPs was increasing continuously over time resulting in a high nanoparticle load after 48 h. The IOH-NP uptake observed in the pH8N8 cells (Fig. 3(a)) was slightly higher (and earlier detectable) than for the AsPC1 cells (Fig. 3(b)). The evidence and high detection capacity of DUT-labelled IOH-NPs *via* confocal microscopy proves that they could also be an effective tool to monitor nanoparticle delivery *in vivo via* NIR-fluorescence imaging.

To evaluate the cytotoxic efficacy of the as-prepared chemotherapeutic IOH-NPs, first of all, *in vitro* studies with single-drug $Gd_2^{3+}[PMX]_3^{2-}$ and $[Gd(OH)]^{2+}[EMP]^{2-}$ IOH-NPs were performed, again, using AsPC1 cells (Fig. 4(a) and (b)) and pH8N8 cells (Fig. 4(c) and (d)). Colorimetric cell viability assays were used to determine the metabolic activity of the respective cells directly after the treatment (0 h) as well as after 24 and 72 h of incubation. Untreated cells incubated with increasing volume (corresponding to the used volumes of the IOH-NPs) of phosphate-buffered saline (PBS) as a negative reference show a strong increase of the metabolic activity corresponding to considerable cell growth the longer the time of incubation (Fig. 4(b) and (c)). In contrast, both single-drug IOH-NPs show a clear concentration-dependent efficacy after 24 and 72 h of treatment. This confirms the chemotherapeutic IOH-NPs not only be effectively internalized by the cells but also evidently release their drug load, resulting in the expected concentration-dependent cytotoxic efficacy. AsPC1 cells turned out to be more affected by $[Gd(OH)]^{2+}[EMP]^{2-}$ (Fig. 4(a)), whereas $Gd_2^{3+}[PMX]_3^{2-}$ shows a higher activity on pH8N8 cells (Fig. 4(d)). Similar behaviour was also observed for the freely dissolved drugs (ESI,† Fig. S12 and S13). It must be noticed that certain absorption of medium, drugs, and nanoparticles occurred (black pillars, Fig. 4 and ESI,† Fig. S12, S13), which needs to be taken into account to evaluate the actual cell growth (indicated by red lines). $Gd_2^{3+}[(PMX)_{0.5}(EMP)_{0.5}]_3^{2-}$ IOH-NPs with chemotherapeutic PMX/EMP cocktail shows clear concentration-dependent efficacy on both AsPC1 and pH8N8 cells (Fig. 4(a) and (d)), which is higher as compared to the single-drug IOH-NPs. Here, it must be noticed that $Gd_2^{3+}[(PMX)_{0.5}(EMP)_{0.5}]_3^{2-}$ IOH-NPs also contain each drug only with half of the concentration as the single-drug IOH-NPs. In comparison to mixtures of the freely dissolved drugs, $Gd_2^{3+}[(PMX)_{0.5}(EMP)_{0.5}]_3^{2-}$ IOH-NPs even result in a slightly reduced cell growth, specifically at low concentrations (5 and 10 μL, ESI,† Fig. S12 and S13). Qualitatively, these observations are

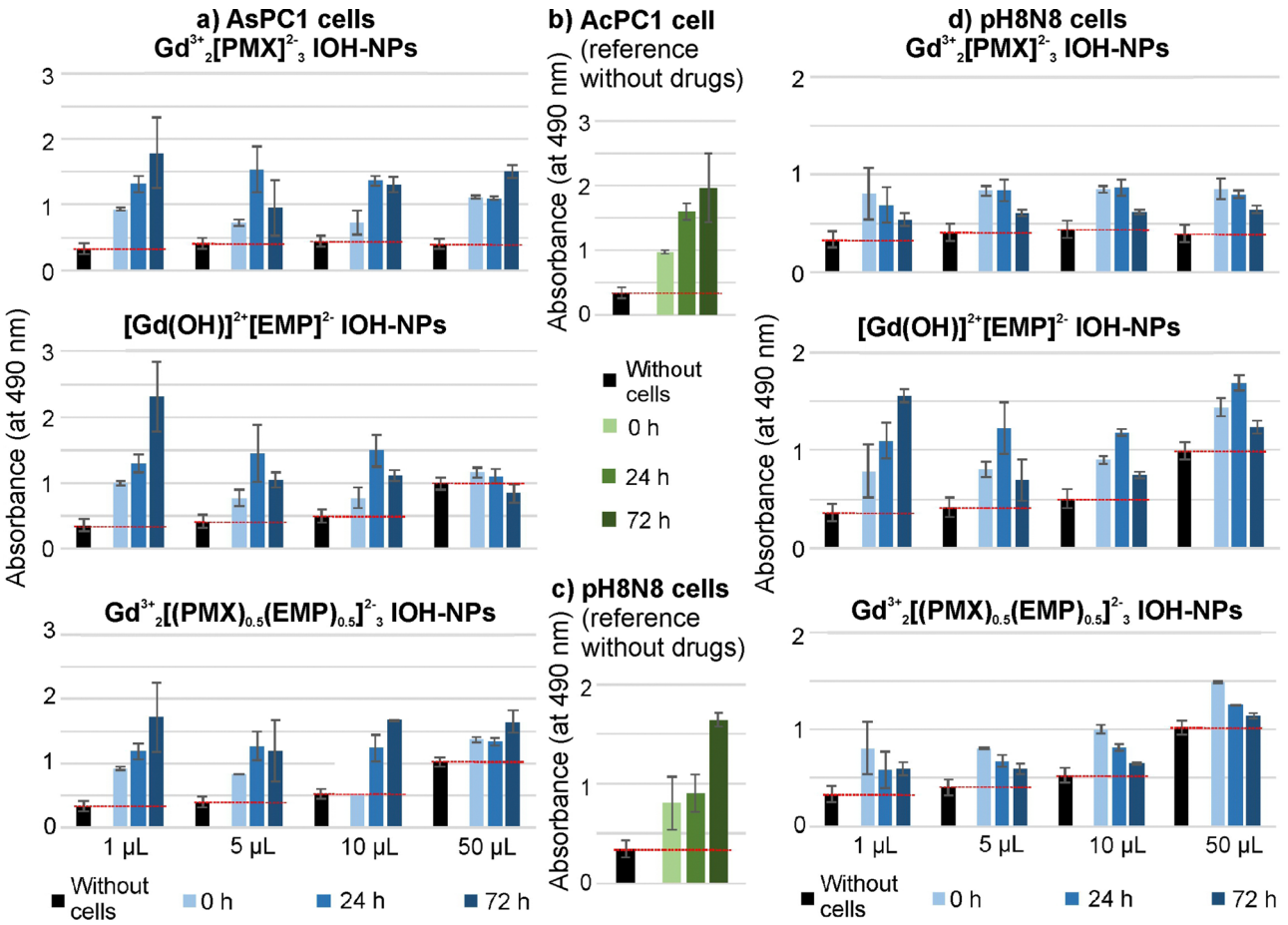

Fig. 4 *In vitro* studies of IOH-NPs with single drug and chemotherapeutic cocktail on (a), (b) AsPC1 and (c), (d) pH8N8 cells. MTT-based viability assay after 0 to 72 h of (a), (d) treatment with the indicated IOH-NP concentrations (0 to 50 μg mL^{-1}) in comparison to (b), (c) untreated cells. The concentration of the freely dissolved drugs was according to their content in the IOH-NPs. Red lines indicate the self-absorption of the medium, and/or drugs and/or IOH-NPs. Error bars correspond to the standard error of n = 4.

also confirmed in cell assays by assessing the confluence using a live-cell analysis system (ESI,† Fig. S14–S21).

The different effects of the IOH-NPs on AsPC1 and pH8N8 tumour cells are not surprising, as these cells originate from different species (human *vs.* mouse), tissues (pancreatic carcinoma *vs.* mammary carcinoma), and as they also exhibit different proliferation rates, chemoresponsiveness, and basal levels of metabolic activity. The delivery of chemotherapeutics *via* nanocarriers has been also already shown to positively affect drug pharmacokinetic by prolonging blood circulation, but also to improve their pharmacodynamics and uptake by tumour tissue.[1–3] Here, nab-Paclitaxel (*i.e.* albumin-nanoparticle-bound paclitaxel) is a prominent example that is already routinely applied in the clinic.[20] The results show that $Gd_2^{3+}[(PMX)_{0.5}(EMP)_{0.5}]_3^{2-}$ IOH-NPs with chemotherapeutic cocktail have high efficacy against different types of tumour cells although they contain a lower concentration of a specific drug as compared to the respective single-drug IOH-NPs. This synergistic effect can be expected to be much stronger in *in vivo* settings than for *in vitro* assays, which are limited by a short duration of the experiment and isolated cell monocultures. *In vivo*, IOH-NPs with a chemotherapeutic cocktail may not only result in an improved tumour treatment but also help to overcome chemotherapy resistance and to reduce side effects, which are the main drawbacks of long-term drug treatments.

3.4 *In vitro* studies with IOH-NPs and cytotoxic cocktail

Whereas the effective formation of reactive oxygen species (ROS) of $Gd_4^{3+}[AlPCS_4]_3^{4-}$ and $La_4^{3+}[TPPS_4]_3^{4-}$ IOH-NPs was

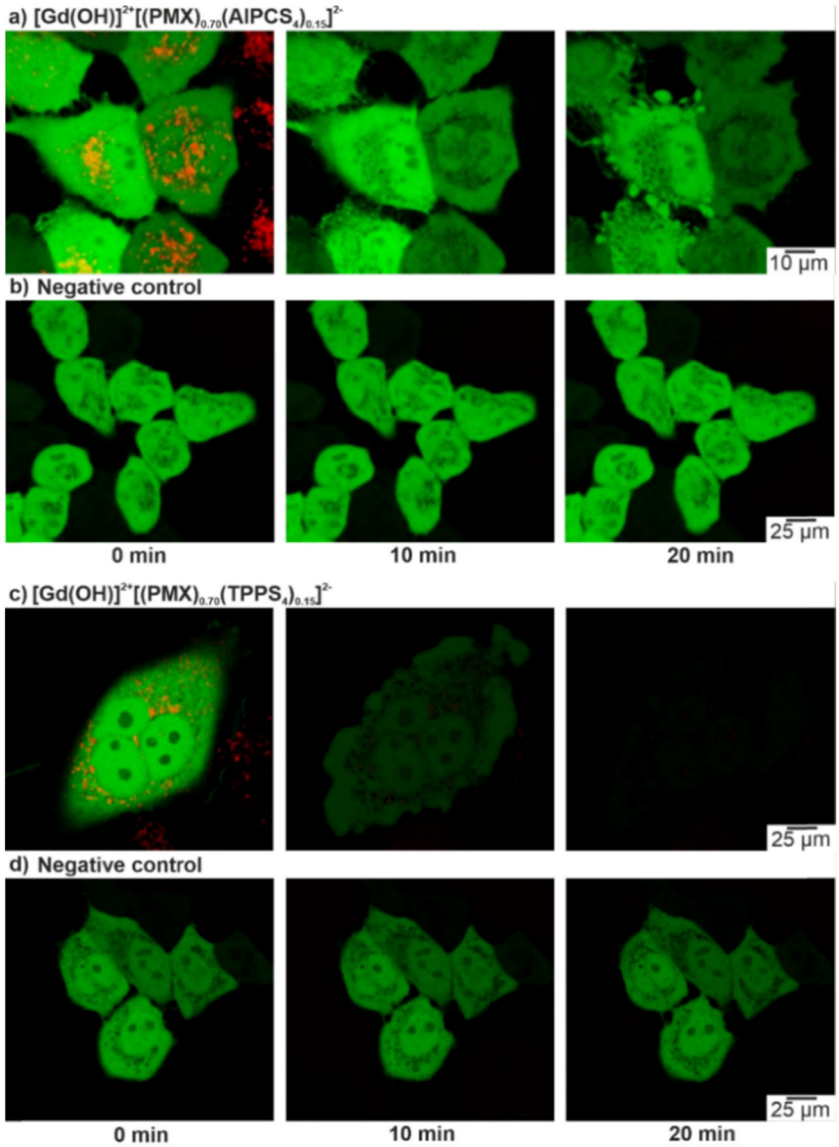

Fig. 5 Confocal microscopy images of HeLa-GFP cells after incubation with $[Gd(OH)]^{2+}[(PMX)_{0.74}(AlPCS_4)_{0.13}]^{2-}$ (a) and $[Gd(OH)]^{2+}[(PMX)_{0.70}(TPPS_4)_{0.15}]^{2-}$ (c) IOH-NPs (50 μg mL^{-1}) for 24 h. Cells were illuminated for 10 and 20 min at 635 nm (for $AlPCS_4$) or at 532 nm (for $TPPS_4$). Untreated HeLa-GFP cells ±illumination are used as negative control (b) and (d). Depicted are the merged images of the fluorescence emission for GFP (λ_{exc} = 488 nm, λ_{em} = 500–540 nm) and the IOH-NPs (λ_{exc} = 635 nm, λ_{em} = 650–750 nm for $AlPCS_4$; λ_{exc} = 532 nm, λ_{em} = 550–650 nm for $TPPS_4$), (identical scale bar for all images in a row).

shown before (ESI,† Fig. S22),[10a,21] dual-drug IOH-NPs with a synergistic cytotoxic and phototoxic effect are presented here for the first time. The activity of $[Gd(OH)]^{2+}[(PMX)_{0.74}(AlPCS_4)_{0.13}]^{2-}$ and $[Gd(OH)]^{2+}[(PMX)_{0.70}(TPPS_4)_{0.15}]^{2-}$ IOH-NPs with a cytostatic cocktail was tested *in vitro* using HeLa-GFP cancer cells. Here, confocal fluorescence microscopy indicates cellular uptake based on the red $AlPCS_4$/$TPPS_4$-derived emission (550–600 nm) of the IOH-NPs, which provides a good contrast against the emission of the green fluorescent protein (GFP) of the cancer cells (Fig. 5(a) and (c)). The intensity of the GFP emission is also coherent with the viability of the cells and shows the activity of intracellular metabolic processes. For this reason, HeLa-GFP cells are also considered as an excellent experimental model to visualize the cytotoxic impact of the $[Gd(OH)]^{2+}[(PMX)_{0.74}(AlPCS_4)_{0.13}]^{2-}$ and $[Gd(OH)]^{2+}[(PMX)_{0.70}(TPPS_4)_{0.15}]^{2-}$ IOH-NPs upon activation by light. The feasibility of the $[Gd(OH)]^{2+}[(PMX)_{0.74}(AlPCS_4)_{0.13}]^{2-}$ and $[Gd(OH)]^{2+}[(PMX)_{0.70}(TPPS_4)_{0.15}]^{2-}$ IOH-NPs for PDT is demonstrated after 10 and 20 min of illumination (635 nm for $AlPCS_4$; 532 nm for $TPPS_4$). Thereafter, the cells show significant changes in their shape and morphology, indicating cell death (Fig. 5(a) and (c)). Moreover, the green emission of the HeLa-GFP cells is significantly reduced after illumination. For $[Gd(OH)]^{2+}[(PMX)_{0.70}(TPPS_4)_{0.15}]^{2-}$, the green emission vanishes almost completely (Fig. 5(c)). This evidences a strong phototoxic effect due to effective ROS generation of the $AlPCS_4$- or $TPPS_4$-containing cytotoxic IOH-NPs compared to untreated cells as negative controls (Fig. 5(b) and (d)). Moreover, the PMX-related cytotoxic activity of IOH-NPs is almost unaffected by illumination (ESI,† Fig. S23).

To provide quantitative results on cell viability after IOH-NP treatment and subsequent illumination, MTT assays were performed (Fig. 6). These experiments were conducted in human colon carcinoma cells (HCT116) and normal human dermal fibroblasts (NHDF), thus, testing not only the cytotoxic impact on cancer cells but also on non-tumour somatic cells of connective tissues. The performance of dividing somatic cells such as fibroblasts is often used to elucidate the therapeutic window for a potential application of a drug with antiproliferative properties such as PMX. For both cell types, the viability

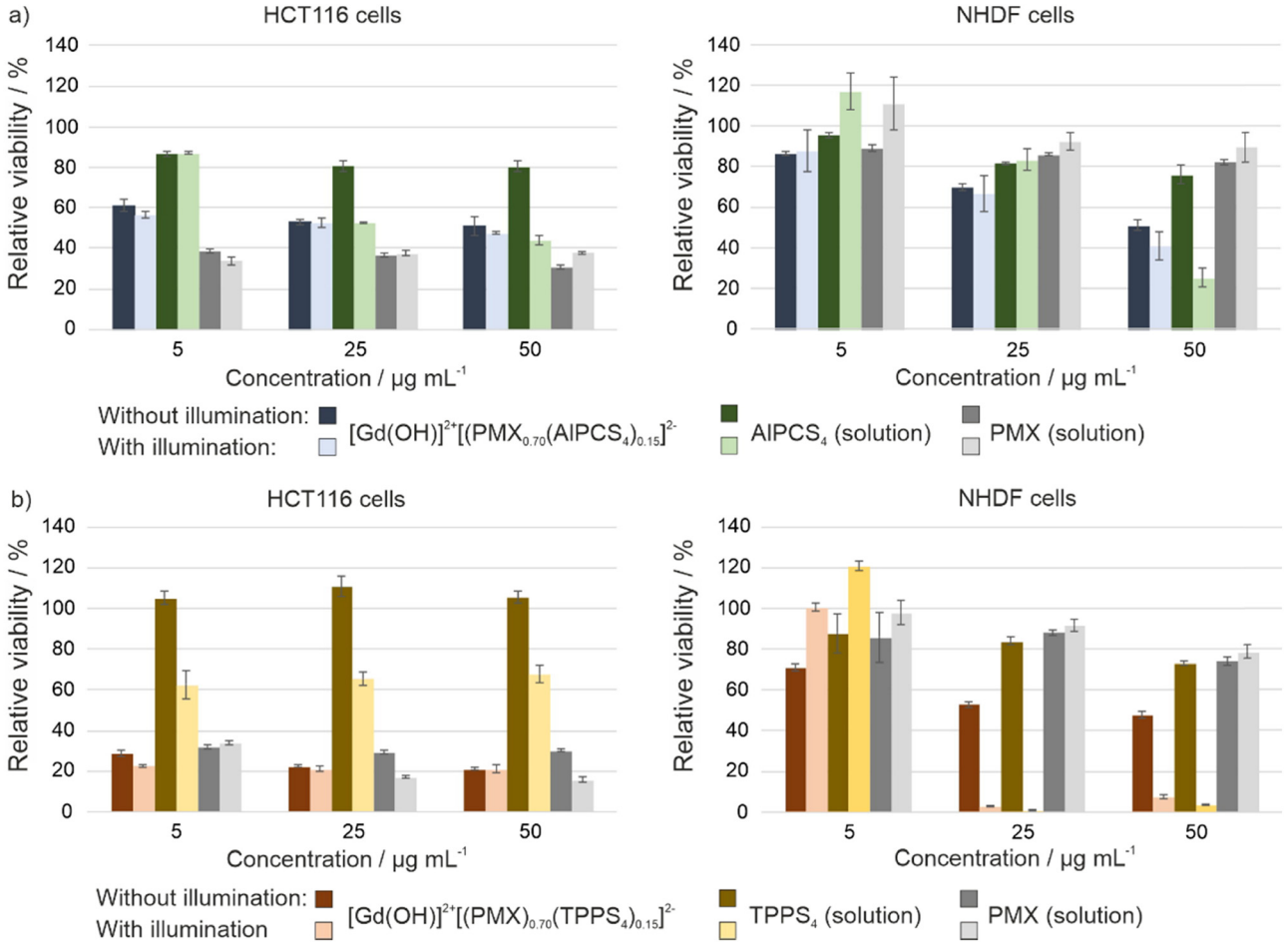

Fig. 6 Cell viability assays with human-colon-carcinoma cells (HCT116) and somatic non-tumour human dermal fibroblasts (NHDF) treated with different concentrations (5, 25, 50 μg mL^{-1}) of $[Gd(OH)]^{2+}[(PMX)_{0.74}(AlPCS_4)_{0.13}]^{2-}$ and $[Gd(OH)]^{2+}[(PMX)_{0.70}(TPPS_4)_{0.15}]^{2-}$ IOH-NPs and the freely dissolved active agents $AlPCS_4$/$TPPS_4$ and PMX (1.6, 7.8, 15.5 μg mL^{-1} $AlPCS_4$; 1.6, 8.0, 16.0 μg mL^{-1} $TPPS_4$; 2.2, 11.0, 22.0 μg mL^{-1} PMX) for 24 h. The concentrations of the freely dissolved agents were according to their dose in the IOH-NPs. Eventually, the cells were illuminated for 30 min at 700 nm (for $AlPCS_4$) or white light ($TPPS_4$) and further incubated for 48 h. The cells were subjected to an MTT assay to determine their viability. The experiments were performed in triplicates. Depicted are the mean values ± SD.

plots provide a comparison of the $[Gd(OH)]^{2+}[(PMX)_{0.74}(AlPCS_4)_{0.13}]^{2-}$ and $[Gd(OH)]^{2+}[(PMX)_{0.70}(TPPS_4)_{0.15}]^{2-}$ IOH-NPs with the freely dissolved $AlPCS_4$/$TPPS_4$ and PMX. The IOH-NPs were applied in concentrations of 5, 25 and 50 μg mL^{-1} and the concentrations of $AlPCS_4$/$TPPS_4$ and PMX were adjusted to their concentration within the IOH-NPs (1.6, 7.8, 15.5 μg mL^{-1} $AlPCS_4$; 1.6, 8.0, 16.0 μg mL^{-1} $TPPS_4$; 2.2, 11.0, 22.0 μg mL^{-1} PMX,). For HCT116 cells, the $[Gd(OH)]^{2+}[(PMX)_{0.74}(AlPCS_4)_{0.13}]^{2-}$ IOH-NPs cause a concentration-dependent effect on the cell viability, which is present but much less expressed than the cytotoxic impact of free PMX in solution (Fig. 6(a) and (b)). A slight photoinduced toxicity can also be observed and becomes more obvious when using higher concentrations of the IOH-NPs. The fact that the HCT116 cells are more affected by the treatment with the IOH-NPs (IC_{50} values of 30 μg mL^{-1} in the dark, 25 μg mL^{-1} after illumination) than NHDF cells (IC_{50} values of 50 μg mL^{-1} in the dark, 43 μg mL^{-1} after illumination) offers a therapeutic window for selective treatment of tumour cells.

Compared to $[Gd(OH)]^{2+}[(PMX)_{0.74}(AlPCS_4)_{0.13}]^{2-}$, the cytotoxic effect of the $[Gd(OH)]^{2+}[(PMX)_{0.70}(TPPS_4)_{0.15}]^{2-}$ IOH-NPs is significantly higher when applied in the same concentration of 5, 25 and 50 μg mL^{-1} (Fig. 6(c) and (d)). The resulting data evidence a decrease in viability of HCT116 cells (IC_{50} values of <5 μg mL^{-1} of IOH-NPs, corresponding to <1.6 μg mL^{-1} of freely dissolved $TPPS_4$) both in the dark and after illumination compared to freely dissolved $TPPS_4$ (IC_{50} values of >16 μg mL^{-1} both in the dark and after illumination). Specifically interesting is that these IOH-NPs outperform the efficiency of free PMX for both cell lines before illumination. The expressed cytotoxicity of the IOH-NPs can be further strengthened upon illumination. Thus, an application of $[Gd(OH)]^{2+}[(PMX)_{0.70}(TPPS_4)_{0.15}]^{2-}$ IOH-NPs at the lowest concentration (5 μg mL^{-1}) decreases the viability of HCT116 cells by more than 70%, whereas the effect on somatic non-tumour cells such as NHDF cells is almost not affected, giving rise to a therapeutic window.

These results demonstrate that both agents the cytotoxic PMX and the photosensitizing $AlPCS_4$ or $TPPS_4$ in the IOH-NPs synergistically contribute to the cell-death initiation and can lead to an improved antitumour performance than the individual therapeutic agents. Furthermore, it should be noticed that the cytotoxicity of the freely dissolved drug PMX has a higher cytotoxic effect by one order of magnitude on HCT116 cells (IC_{50} <2.2 μg mL^{-1}) than on NHDF cells (IC_{50} >22 μg mL^{-1}). Finally, it needs to be noticed that the cytotoxic effect of freely dissolved PMX alone is not illumination dependent. This finding also confirms that PMX is not considerably degraded upon illumination.

Angiogenesis – *i.e.* the formation of new blood vessels – plays a crucial role in tumour progression since tumour growth strongly depends on the oxygen and nutrient supply. Therefore, inhibition or disruption of angiogenesis is considered as an efficient way of antineoplastic treatment.[22] In this regard, the angiogenesis-inhibiting effect proven for several porphyrin- and phthalocyanine-based photosensitizers is a specific advantage of PDT.[23] This effect is mainly based on an altering of the morphological properties of the blood vessels, which causes vasoconstriction and permeabilization of the microvasculature.[24] The resulting lack of oxygen directly leads to the inhibition of tumour growth. For this reason, experiments with $[Gd(OH)]^{2+}[(PMX)_{0.74}(AlPCS_4)_{0.13}]^{2-}$ and $[Gd(OH)]^{2+}[(PMX)_{0.70}(TPPS_4)_{0.15}]^{2-}$ IOH-NPs were performed in human umbilical vein endothelial cells (HUVEC) (Fig. 7). Cells were seeded on a vascular endothelial growth factor-containing matrix (Geltrex). After incubation with the IOH-NPs and subsequent illumination, the cells were examined in comparison to cells treated with the freely dissolved photosensitizers alone (positive controls) and untreated cells (negative controls). For the evaluation of the tubular integrity *via* confocal fluorescent microscopy, the cell nuclei of the endothelial cells were stained with Hoechst 33342. For the IOH-NP-treated samples, the endothelial cell alignment and microcapillary formation were not affected in comparison to the negative controls (Fig. 7). However, after illumination (at 700 nm for $AlPCS_4$ and white light for $TPPS_4$), the $[Gd(OH)]^{2+}[(PMX)_{0.74}(AlPCS_4)_{0.13}]^{2-}$- and $[Gd(OH)]^{2+}[(PMX)_{0.70}(TPPS_4)_{0.15}]^{2-}$-treated samples show a total suppression of the microcapillary network. The effect is even stronger as compared to freely dissolved $H_4(AlPCS_4)$/$H_4(TPPS_4)$ as positive controls.

In sum, these findings clearly demonstrate that angiogenesis can be selectively inhibited by the IOH-NPs with cytotoxic and phototoxic properties. The phototoxic effect initiated by the photosensitizer is equaled to the free photosensitizers$AlPCS_4$/$TPPS_4$ showing that the incorporation of the photosensitizer into the IOH-NPs is not decreasing its phototoxicity. In contrast, the contribution of PMX to the inhibition of the angiogenesis can be neglected as freely dissolved PMX at similar concentrations (2.2–22 μg mL^{-1}) has almost no effect (decrease $<15\%$) on the viability of HUVEC after 72 h of treatment as observed *via* MTT assays (ESI,† Fig. S24 and S25). This enables the IOH-NPs for selective destruction of the tumour microvasculature *via* their photoinduced cytotoxicity.

3.5 Effect of IOH-NPs on 3D tumour spheroids

To examine the cytotoxicity and the anti-proliferative effect of the IOH-NPs on 3D cell cultures, 3D tumour spheroids were generated and treated with the respective IOH-NPs. Here, HepG2 spheroids were used as they show a uniform spherical structure. In regard to the chemotherapeutic IOH-NPs, $Gd_2{}^{3+}[PMX]_3{}^{2-}$ did not show a noticeable effect on the spheroids, whereas $[Gd(OH)]^{2+}[EMP]^{2-}$ strongly suppresses its growth (Fig. 8(a)). Both single-drug IOH-NPs behave more-or-less similar to the freely dissolved drugs PMX and EMP, with $[Gd(OH)]^{2+}[EMP]^{2-}$ IOH-NPs showing an even stronger effect than free EMP. The chemotherapeutic cocktail in $Gd_2{}^{3+}[(PMX)_{0.5}(EMP)_{0.5}]_3{}^{2-}$ also shows high efficacy on the spheroids. Notably, $Gd_2{}^{3+}[(PMX)_{0.5}(EMP)_{0.5}]_3{}^{2-}$ contains only 50% of the dose of the more active EMP than single-drug $[Gd(OH)]^{2+}[EMP]^{2-}$. Due to three-dimensional growth, higher density and limited diffusion, the cytotoxic effect on spheroids is observed at higher concentrations ($\geq$100 μg mL^{-1}, Fig. 8) as for cells ($\geq$10 μg mL^{-1}, Fig. 4). However, this higher dose is required for the IOH-NPs as well as for the freely dissolved drugs. For the cyto-/phototoxic IOH-NPs $[Gd(OH)]^{2+}[(PMX)_{0.74}(AlPCS_4)_{0.13}]^{2-}$ and $[Gd(OH)]^{2+}[(PMX)_{0.70}(TPPS_4)_{0.15}]^{2-}$, a cytostatic effect without

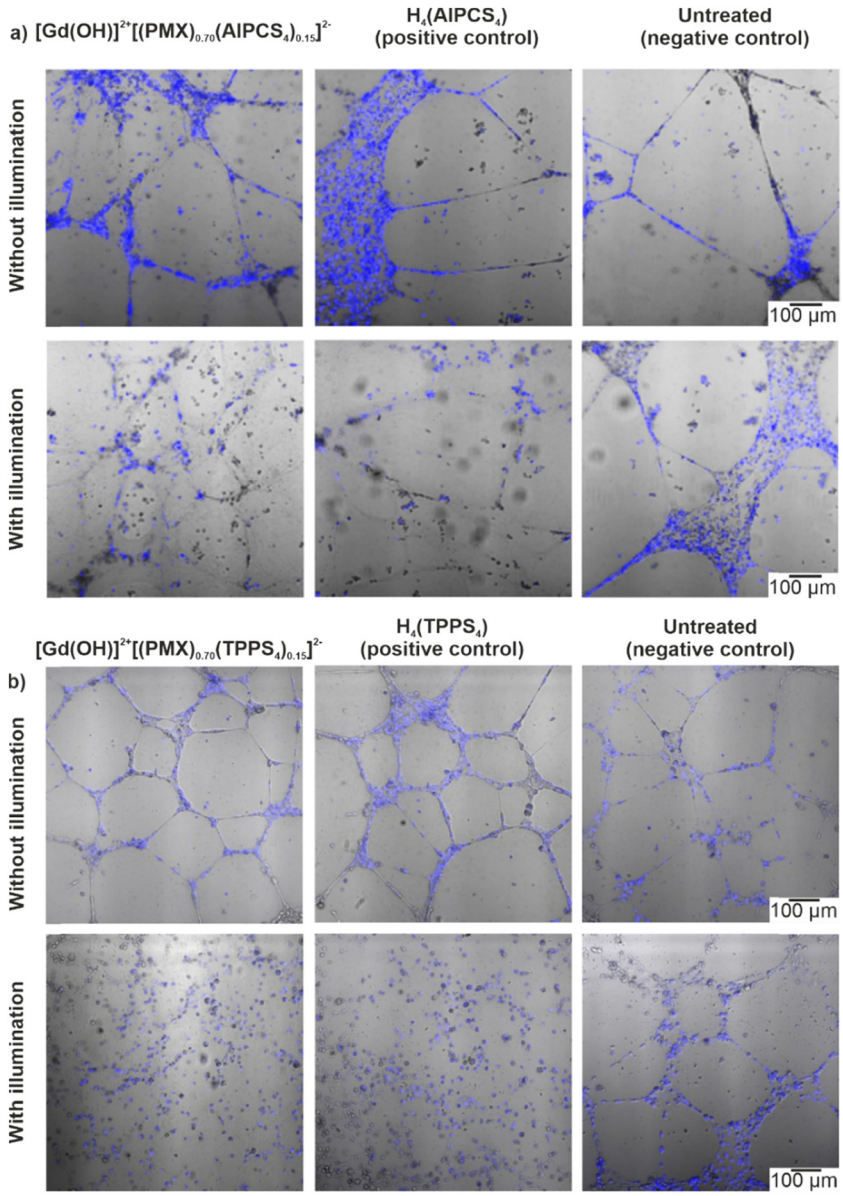

Fig. 7 Impact of $[Gd(OH)]^{2+}[(PMX)_{0.74}(AlPCS_4)_{0.13}]^{2-}$ (a) and $[Gd(OH)]^{2+}[(PMX)_{0.70}(TPPS_4)_{0.15}]^{2-}$ (b) IOH-NPs (50 µg mL^{-1}) on angiogenesis of human umbilical vein endothelial cells (HUVEC) upon illumination with 700 nm light ($AlPCS_4$, 40 min) and white light ($TPPS_4$, for 3 min) in comparison to cells treated with the freely dissolved photosensitizers $H_4(AlPCS_4)$ (15.5 µg mL^{-1}) and $H_4(TPPS_4)$ (16.0 µg mL^{-1}) and non-treated HUVEC (negative controls). Depicted are the fluorescence confocal microscopy images of cells treated with Hoechst 33342 (2 µg mL^{-1}) to visualize cell nuclei (λ_{exc} = 405 nm, λ_{em} = 410–450 nm) merged with the brightfield image (identical scale bar for all images in a row).

illumination (due to PMX/EMP) as well as an additional phototoxic effect after illumination (due to $AlPCS_4$/$TPPS_4$) is obvious (Fig. 8(b)). The phototoxic effect is generally more pronounced for PMX-based samples, since the cytostatic effect of PMX on HepG2 spheroids is lower than for EMP. Combining chemotherapeutics and photosensitizers in IOH-NPs in any case results in a stronger cytostatic effect than illumination of freely dissolved photosensitizers alone.

Cytotoxicity was also demonstrated by live/death staining of the spheroids after 24 h of incubation with the IOH-NPs or the respective freely dissolved agents (Fig. 9). For this purpose, living cells were stained with the fluorescent dye calcein AM (green), whereas dead cells were labelled with propidium iodide (PI, red). For the chemotherapeutic IOH-NPs, again, the efficacy of $[Gd(OH)]^{2+}[EMP]^{2-}$ on HepG2 spheroids is higher than for $Gd_2^{3+}[PMX]_3^{2-}$. Interestingly, freely dissolved PMX and EMP have a lower toxic effect on the spheroids after 24 h than the respective IOH-NPs (Fig. 9(a)). The latter holds also for $Gd_2^{3+}[(PMX)_{0.5}(EMP)_{0.5}]_3^{2-}$ IOH-NPs in comparison to a mixture of freely dissolved PMX and EMP. For the phototoxic systems, live/dead staining shows that – despite a pronounced phototoxicity of freely dissolved $AlPCS_4$/$TPPS_4$ – $[Gd(OH)]^{2+}[(PMX)_{0.74}(AlPCS_4)_{0.13}]^{2-}$ and $[Gd(OH)]^{2+}[(PMX)_{0.70}(TPPS_4)_{0.15}]^{2-}$ IOH-NPs exhibit a higher phototoxic effect as well as an additional

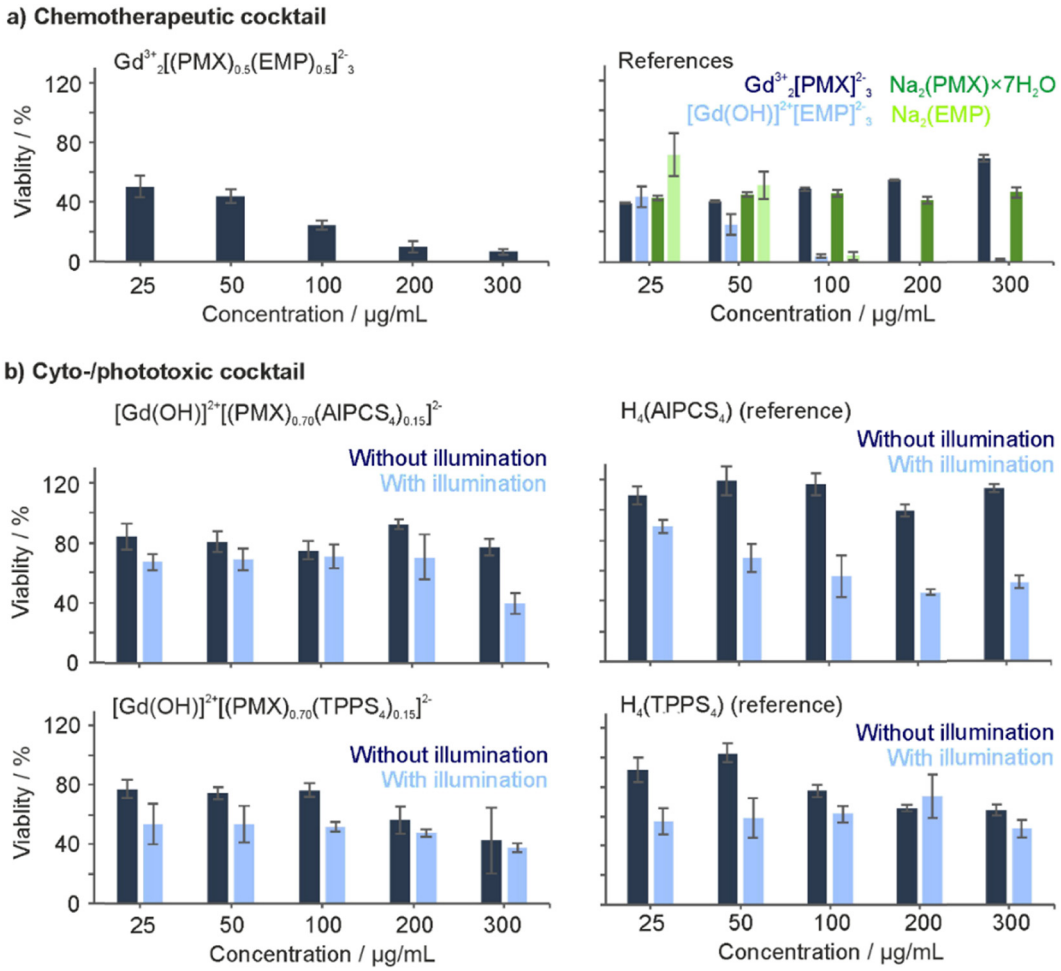

Fig. 8 Cell viability assays with HepG2 tumour spheroids treated with different concentrations (25, 50, 100, 200, 300 µg mL^{-1}) of (a) chemotherapeutic $Gd_2^{3+}[PMX]_3^{2-}$, $[Gd(OH)]^{2+}[EMP]^{2-}$, and $Gd_2^{3+}[(PMX)_{0.5}(EMP)_{0.5}]_3^{2-}$ IOH-NPs as well as (b) cyto-/phototoxic $[Gd(OH)]^{2+}[(PMX)_{0.74}(AlPCS_4)_{0.13}]^{2-}$ and $[Gd(OH)]^{2+}[(PMX)_{0.70}(TPPS_4)_{0.15}]^{2-}$ IOH-NPs with the freely dissolved agents as references (PMX with 28.13, 56.25, 112.5, 225.0, 337.5 µg mL^{-1}; EMP with 19.75, 39.5, 79.0, 158.0, 237.0 µg mL^{-1}; $AlPCS_4$ with 7.75, 15.5, 31.0, 62.0, 93.0 µg mL^{-1}; $TPPS_4$ with 8.0, 16.0, 32.0, 64.0, 96.0 µg mL^{-1}) for 24 h. The concentrations of the freely dissolved agents were according to their dose in the IOH-NPs. Eventually, the cells were illuminated for 30 min at a wavelength of 700 nm (for $AlPCS_4$) or white light (for $TPPS_4$) and further incubated for 48 h. The experiments were performed in triplicates. Depicted are their mean values ±SD.

cytostatic effect without illumination (Fig. 9(b)). Finally, the IOH-NPs have a more uniform effect on the entire spheroid, whereas the toxicity of the freely dissolved agents is more restricted to the center of the spheroids. This is probably due to the penetration properties of the freely dissolved drugs, which show an increased concentration in the interior of the spheroids, whereas the IOH-NPs are evenly distributed all over the spheroid (Fig. 10).

The anti-proliferation effect of the IOH-NPs on the growth of 3D cell cultures was further evaluated by monitoring the proliferation of HepG2 spheroids for 7 days (Fig. 11 and ESI,† Fig. S26, S27). Generally, the size of all tumour spheroids treated with any type of IOH-NPs decreased after 3 days. Furthermore, IOH-NPs containing EMP – $[Gd(OH)]^{2+}[EMP]^{2-}$ and $Gd_2^{3+}[(PMX)_{0.5}(EMP)_{0.5}]_3^{2-}$ – show dissolution of the spheroids after only 3 days (Fig. 11(a) and ESI,† Fig. S26). Freely dissolved PMX did not have any dissolving effect on the spheroid and only reduces its growth. Spheroids treated with the cyto-/phototoxic IOH-NPs $[Gd(OH)]^{2+}[(PMX)_{0.74}(AlPCS_4)_{0.13}]^{2-}$ and $[Gd(OH)]^{2+}[(PMX)_{0.70}(TPPS_4)_{0.15}]^{2-}$ after illumination also show dissolution of the spheroids but only after 7 days of incubation (Fig. 11(b) and ESI,† Fig. S27). The freely dissolved photosensitizing agents $H_4(AlPCS_4)$/$H_4(TPPS_4)$ caused similar morphological changes in the spheroids after illumination, whereas the treated but non-illuminated spheroids continued to grow at similar rates to the untreated control.

In sum, 3D cell cultures with HepG2 spheroids show that IOH-NPs with a cocktail of active agents develop the effect of every single agent. This proves the effective uptake of the IOH-NPs and the release of the chemotherapeutic drugs. IOH-NPs show a more uniform distribution in spheroids and an efficacy that may even exceed that of single agents. The IOH-NP-mediated accumulation of different chemotherapeutic and/or photosensitizing agents in tumour tissue is specifically promising in the complex organism to guarantee an optimal result of chemotherapy.

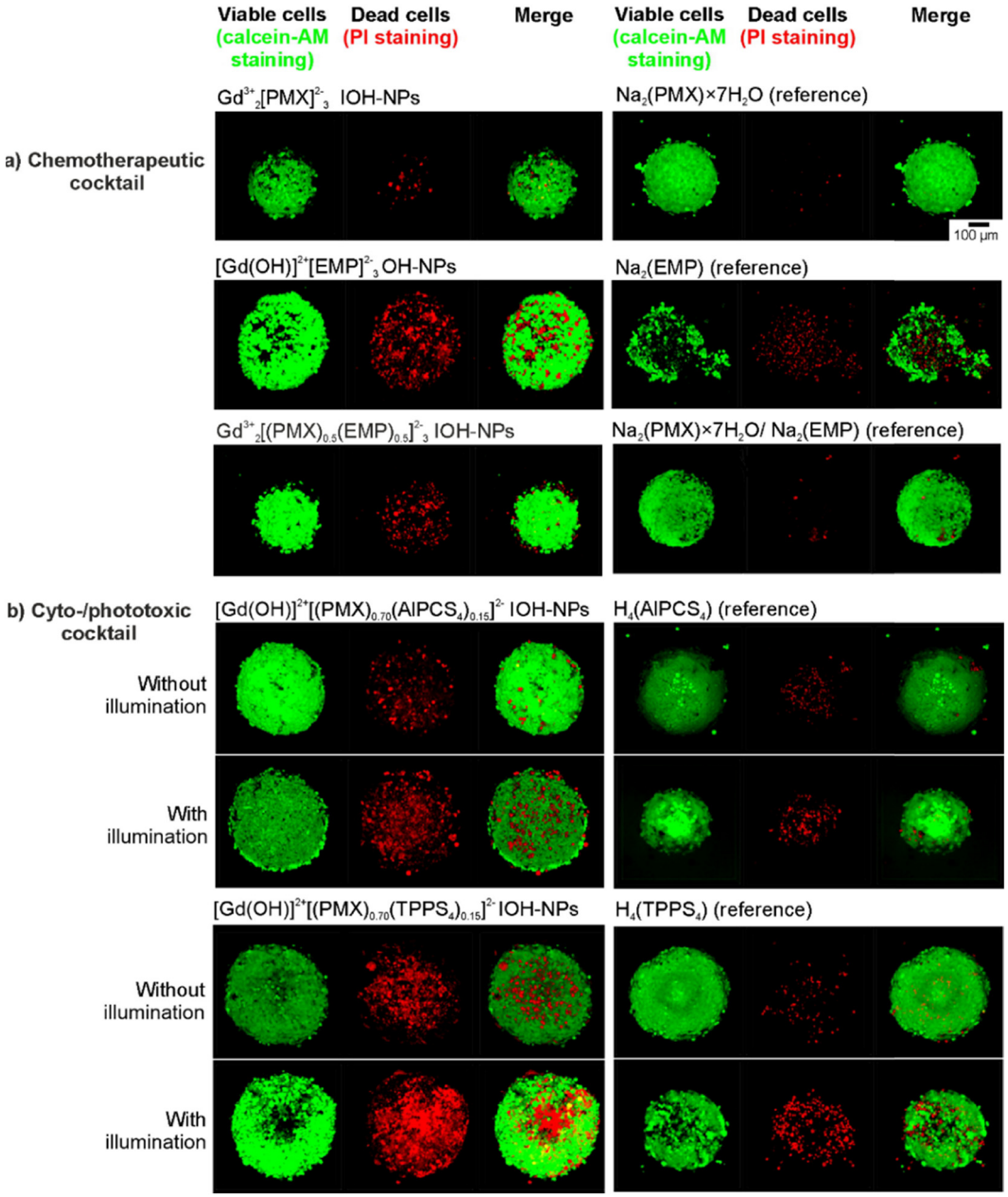

Fig. 9 Live/dead cell assay on HepG2 tumour spheroids: 3D confocal microscopy of spheroids treated for 48 h with 100 µg mL^{-1} of (a) $Gd_2^{3+}[PMX]_3^{2-}$, $[Gd(OH)]^{2+}[EMP]^{2-}$, and $Gd_2^{3+}[(PMX)_{0.5}(EMP)_{0.5}]_3^{2-}$ IOH-NPs (PMX with 112.5 µg mL^{-1}, EMP with 79.0 µg mL^{-1} as references) as well as of (b) $[Gd(OH)]^{2+}[(PMX)_{0.74}(AlPCS_4)_{0.13}]^{2-}$ and $[Gd(OH)]^{2+}[(PMX)_{0.70}(TPPS_4)_{0.15}]^{2-}$ IOH-NPs ($AlPCS_4$ with 31 µg mL^{-1}, $TPPS_4$ with 32 µg mL^{-1} as references). Illumination of photosensitizing compounds after 24 h for 30 min at 700 nm (for $AlPCS_4$) or with white light (for $TPPS_4$). Spheroids were stained with Calcein AM (green; λ_{exc} = 494 nm, λ_{em} = 500–580 nm) for viable cells and propidium iodide (PI, red; λ_{exc} = 532 nm, λ_{em} = 610–700 nm) for dead cells (identical scale bar for all images).

4. Conclusions

The material concept of the inorganic–organic hybrid nanoparticles (IOH-NPs) was expanded for the first time to IOH-NPs with a cocktail of at least two active agents with high loading. Specifically, $Gd_2^{3+}[(PMX)_{0.5}(EMP)_{0.5}]_3^{2-}$ with a chemotherapeutic cocktail (PMX: pemetrexed, EMP: estramustine phosphate) and $[Gd(OH)]^{2+}[(PMX)_{0.74}(AlPCS_4)_{0.13}]^{2-}$ and $[Gd(OH)]^{2+}[(PMX)_{0.70}(TPPS_4)_{0.15}]^{2-}$ with a combination of cytotoxic and photosensitizing agents ($AlPCS_4$: aluminum(III) chlorido phthalocyanine tetrasulfonate, $TPPS_4$: tetraphenylporphine sulfonate) were realized. Generally, these IOH-NPs are characterized by a simple synthesis in water, particle diameters of 40 to 60 nm, high colloidal stability in water due to negative surface charging and an unprecedented high load of active agents with 71 to 82% of the total nanoparticle mass. Furthermore, they are enabled for fluorescence-based monitoring and show deep-red emission, which is well suitable for nanoparticle monitoring.

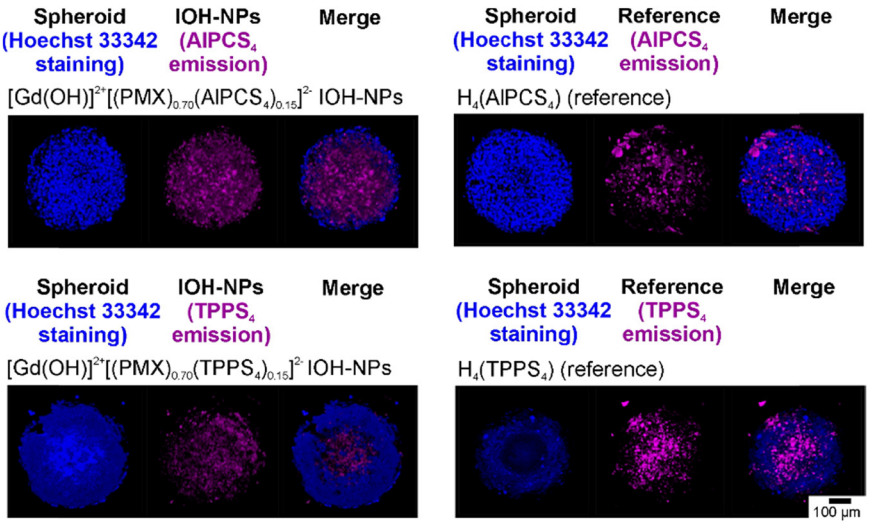

Fig. 10 3D-Confocal microscopy of HepG2 tumour spheroids after 24 h treatment with 100 µg mL^{-1} of $[Gd(OH)]^{2+}[(PMX)_{0.74}(AlPCS_4)_{0.13}]^{2-}$ and $[Gd(OH)]^{2+}[(PMX)_{0.70}(TPPS_4)_{0.15}]^{2-}$ IOH-NPs ($AlPCS_4$ with 31 µg mL^{-1}, $TPPS_4$ with 32 µg mL^{-1} as references). Hoechst 33342 (2 µg mL^{-1}) was used for nuclear staining. Merged images of fluorescence emission for IOH-NPs (purple; λ_{exc} = 635 nm, λ_{em} = 650–750 nm for $AlPCS_4$, λ_{exc} = 532 nm, λ_{em} = 550–650 nm for $TPPS_4$) and Hoechst (blue; λ_{exc} = 405 nm, λ_{em} = 410–450 nm) (identical scale bar for all images).

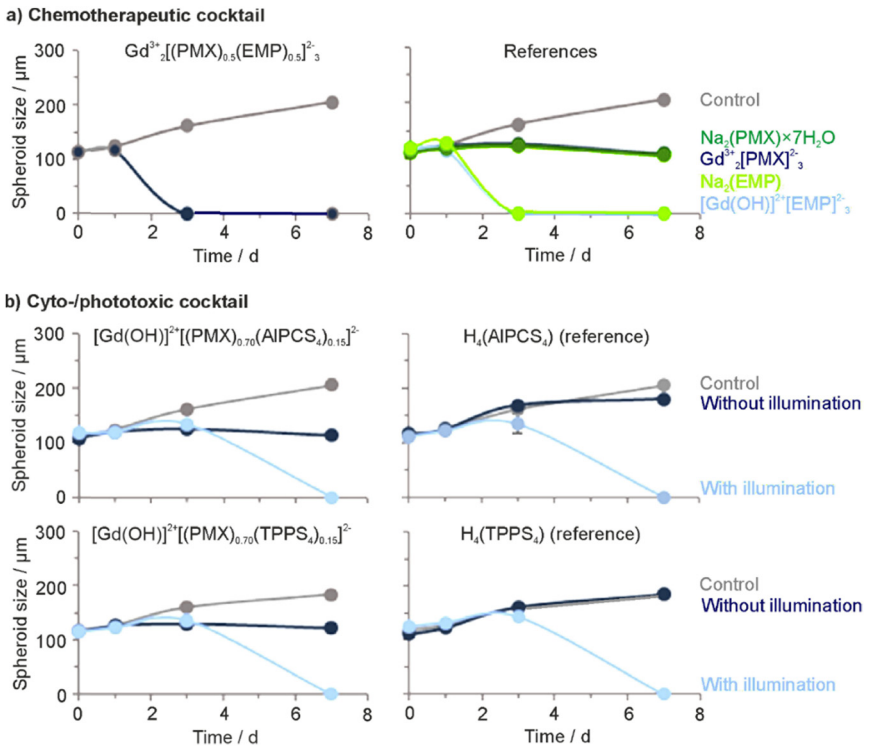

Fig. 11 Measurement of HepG2 spheroid growth before treatment and 1, 3, and 7 days after treatment. Spheroids were treated with 100 µg mL^{-1} of (a) $Gd_2^{3+}[PMX]_3^{2-}$, $[Gd(OH)]^{2+}[EMP]^{2-}$, and $Gd_2^{3+}[(PMX)_{0.5}(EMP)_{0.5}]_3^{2-}$ IOH-NPs (PMX with 112.5 µg mL^{-1}, EMP with 79.0 µg mL^{-1} as references) as well as of (b) $[Gd(OH)]^{2+}[(PMX)_{0.74}(AlPCS_4)_{0.13}]^{2-}$ and $[Gd(OH)]^{2+}[(PMX)_{0.70}(TPPS_4)_{0.15}]^{2-}$ IOH-NPs ($AlPCS_4$ with 31 µg mL^{-1}, $TPPS_4$ with 32 µg mL^{-1} as references). The concentrations of the freely dissolved agents were according to their dose in the IOH-NPs. Illumination of photosensitizing compounds for 30 min at 700 nm (for $AlPCS_4$) or with white light (for $TPPS_4$) and further incubated for 48 h. Size change of HepG2 tumour spheroids compared to the control group during the 7 day treatment in (a). Morphological change of spheroids during the 7 day treatment in (b). Values expressed as the mean ± SD (n = 6).

IOH-NPs with chemotherapeutic/cytostatic cocktail outperform single-agent IOH-NPs and freely dissolved agents as references throughout. Thus, in a murine-breast-cancer cell line (pH8N8 cells), IOH-NPs with a chemotherapeutic PMX/

EMP cocktail exhibit a more than 2-times higher activity than the respective single-drug IOH-NPs. For IOH-NPs with combined cytotoxic and photosensitizing agents, illumination of HeLa-GFP cancer cells displays effective ROS formation with a considerable phototoxic effect. MTT assays with a variety of human tumour and somatic non-cancerogenic cells such as colon cancer cells (HCT116), HepG2 cells, human dermal fibroblasts (NHDF) and human umbilical vein endothelial cells (HUVECs) prove the cytotoxic and even additive effect of the IOH-NPs on cancer cells, whereas somatic cells of connective tissues are only affected at very high concentrations. Angiogenesis with human umbilical vein endothelial cells (HUVEC) shows a total suppression of the microcapillary network after incubation with the IOH-NPs and illumination (for $AlPCS_4$ 40 min with red light, for $TPPS_4$ 3 min with white light), which clearly outperforms the freely dissolved $H_4(AlPCS_4)$/$H_4(TPPS_4)$ photosensitizers. Toxicity and anti-proliferation studies on 3D tumour spheroids with human liver cancer cells (HepG2) confirm the results from 2D cell cultures with superior distribution and activity of IOH-NPs with a chemotherapeutic or cytostatic cocktail over single-drug IOH-NPs and freely dissolved drugs. Altogether, IOH-NPs with chemotherapeutic/cytostatic cocktail outperform the respective single-agent IOH-NPs and show a strong synergistic effect due to the combination of active agents. Such adjunctive approaches are highly relevant in clinics to overcome chemotherapy resistance and metastasis. In fact, IOH-NPs as a platform concept offer even more flexibility to select and to combine also other drugs and drug cocktails in order to address specific disease patterns.

Conflicts of interest

The authors declare no competing financial interests.

Acknowledgements

M. K., A. M., J. P., U. S., C. F. thank the Deutsche Forschungsgemeinschaft (DFG) for funding within the Research Training Group 2039. Moreover, M. K., J. N., F. A. and C. F. are grateful to the DFG for funding within the project ''Synergistic Image-guided Nanoparticles for Drug Delivery (SIN-Drug)''. M. K. is also thankful to the Studienstiftung des Deutschen Volkes for the scholarship. J. P. also thanks the Ministerium für Ernährung, Ländlichen Raum und Verbraucherschutz Baden-Württemberg (MLR) for financial support. U. S. thanks for funding under Germany's Excellence Strategy ***via*** the Excellence Cluster ''3D Matter Made to Order (EXC-2082/1-390761711)''. The work of A. M., J. P., J. S., and U. S. was also supported by the Helmholtz Program Materials Systems Engineering (MSE). Finally, M. K., C. F., and U. S. thank Henriette Gröger and Jacqueline Stier for their excellent assistance in experiments.

References

1 (*a*) F. Farjadian, A. Ghasemi, O. Gohari, A. Roointan, M. Karimi and M. R. Hamblin, *Nanomedicine*, 2019, **14**, 93–126; (*b*) D. Peer, J. M. Karp, S. Hong, O. C. Farokhzad, R. Margalit and R. Langer, *Nat. Nanotechnol.*, 2007, **2**, 751–760.

2 (*a*) Y. Barenholz, *J. Controlled Release*, 2012, **160**, 117–134; (*b*) W. J. Gradishar, S. Tjulandin, N. Davidson, H. Shaw, D. Heather, N. Desai, P. Bhar, M. Hawkins and J. O'Shaughnessy, *J. Clin. Oncol.*, 2005, **23**, 7794–7803.

3 (*a*) S. Kunjachan, J. Ehling, G. Storm, F. Kiessling and T. Lammers, *Chem. Rev.*, 2015, **115**, 10907–10937; (*b*) T. L. Doane and C. Burda, *Chem. Soc. Rev.*, 2012, **41**, 2885–2911.

4 (*a*) K. Ulbrich, K. Hola, V. Subr, A. Bakandritsos, J. Tucek and R. Zboril, *Chem. Rev.*, 2016, **116**, 5338–5431; (*b*) E. Blanco, H. Shen and M. Ferrari, *Nat. Biotechnol.*, 2015, **33**, 941–951.

5 (*a*) D. Shi, D. Beasock, A. Fessler, J. Szebeni, J. Y. Ljubimova, K. A. Afonin and M. A. Dobrovolskaia, *Adv. Drug Delivery Rev.*, 2022, **180**, 114079; (*b*) B. Ghosh and S. Biswas, *J. Controlled Release*, 2021, **332**, 127–147; (*c*) S. E. Birk, A. Boisen and K. H. Nielsen, *Adv. Drug Delivery Rev.*, 2021, **174**, 30–52; (*d*) C. D. Spicer, C. Jumeaux, B. Gupta and M. M. Stevens, *Chem. Soc. Rev.*, 2018, **47**, 3574–3620; (*e*) M. Dangol, H. Yang, C. G. Li, S. F. Lahiji, S. Kim, Y. Ma and H. Jung, *J. Controlled Release*, 2016, **223**, 118–125; (*f*) C. E. Wang, P. S. Stayton, S. H. Pun and A. J. Convertine, *J. Controlled Release*, 2015, **219**, 345–354; (*g*) M. Talelli, M. Barz, C. J. F. Rijcken, F. Kießling, W. E. Hennink and T. Lammers, *Nano Today*, 2015, **10**, 93–117; (*h*) D. Ma, G. Hettiarachchi, D. Nguyen, B. Zhang, J. B. Wittenberg, P. Y. Zavalij, V. Briken and L. Isaacs, *Nat. Chem.*, 2012, **4**, 503–510.

6 (*a*) X.-H. Cao, M.-X. Liang, Y. Wu, K. Yang, J.-H. Tang and W. Zhang, *Nanomedicine*, 2021, **16**, 1519–1537; (*b*) M. Abri Aghdam, R. Bagheri, J. Mosafer, B. Baradaran, M. Hashemzaei, A. Baghbanzadeh, M. de la Guardia and A. Mokhtarzadeh, *J. Controlled Release*, 2019, **315**, 1–22; (*c*) X. Liu, F. Wu, Y. Ji and L. Yin, *Bioconjugate Chem.*, 2019, **30**, 305–324; (*d*) H. Cabral and K. Kataoka, *J. Controlled Release*, 2014, **190**, 465–476.

7 (*a*) A. Jozefczak, K. Kaczmarek and R. Bielas, *Theranostics*, 2021, **11**, 10091–10113; (*b*) H. Huang, W. Feng, Y. Chen and J. Shi, *Nano Today*, 2020, **35**, 100972; (*c*) J. Liu, J. Dong, T. Zhang and Q. Peng, *J. Controlled Release*, 2018, **286**, 64–73; (*d*) J.-J. Hu, D. Xiao and X. Z. Zhang, *Small*, 2016, **12**, 3344–3359; (*e*) A. B. Satterlee and L. Huang, *Theranostics*, 2016, **6**, 918–929; (*f*) D. Ling, N. Lee and T. Hyeon, *Acc. Chem. Res.*, 2015, **48**, 1276–1285; (*g*) A. K. Gupta and M. Gupta, *Biomater.*, 2005, **26**, 3995–4021; (*h*) C. Barbe, J. Bartlett, L. Kong, K. Finnie, H. Q. Lin, M. Larkin, S. Calleja, A. Bush and G. Calleja, *Adv. Mater.*, 2004, **16**, 1959–1966.

8 (*a*) K. Yang, Z. Yang, G. Yu, Z. Nie, R. Wang and X. Chen, *Adv. Mater.*, 2022, **34**, 210743; (*b*) Q. Pei, X. Hu, X. Zheng, S. Liu, Y. Li, X. Jing and Z. Xie, *ACS Nano*, 2018, **12**, 1630–1641.

9 B. Shrestha, L. Wang, E. M. Brey, G. Romero Uribe and L. Tang, *Pharmaceutics*, 2021, **13**, 853.

10 (*a*) B. L. Neumeier, M. Khorenko, F. Alves, O. Goldmann, J. Napp, U. Schepers, H. M. Reichardt and C. Feldmann, *ChemNanoMat*, 2018, **4**, 1–23; (*b*) J. G. Heck, J. Napp, S. Simonato, J. Möllmer, M. Lange, H. R. Reichardt, R. Staudt, F. Alves and C. Feldmann, *J. Am. Chem. Soc.*, 2015, **137**, 7329–7336.

11 (*a*) J. Napp, M. A. Markus, J. G. Heck, C. Dullin, W. Möbius, D. Gorpas, C. Feldmann and F. Alves, *Theranostics*, 2018, **4**, 1–23; (*b*) J. G. Heck, K. Rox, H. Lünsdorf, T. Lückerath, N. Klaassen, E. Medina, O. Goldmann and C. Feldmann, *ACS Omega*, 2018, **3**, 8589–8594.

12 (*a*) O. Sartor and J. S. de Bono, *New Engl. J. Med.*, 2018, **378**, 645–657; (*b*) K. D. Rollins and C. Lindley, *Clin. Ther.*, 2005, **27**, 1343–1382; (*c*) V. J. Sinibaldi, M. A. Carducci, S. Moore-Cooper, M. Laufer, M. Zahurak and M. A. Eisenberger, *Cancer*, 2002, **94**, 1457–1465.

13 (*a*) H. Abrahamse and M. R. Hamblin, *Biochem. J.*, 2016, **473**, 347–364; (*b*) R. Bonnett, *Chem. Soc. Rev.*, 1995, **24**, 19–33.

14 V. K. LaMer and R. H. J. Dinegar, *J. Am. Chem. Soc.*, 1950, **72**, 4847–4854.

15 V. Rein, E. Zittel, K. Hagens, N. Redinger, U. Schepers, H. Mehlhorn, U. Schaible and C. Feldmann, *Adv. Funct. Mater.*, 2019, **29**, 1900543.

16 R. Jog and D. J. Burgess, *J. Pharm. Sci.*, 2017, **106**, 39–65.

17 (*a*) W. Pawlina and M. A. Ross, *Histology: A Text and Atlas*, 8th edn, Walters Kluwer, Philadelphia, 2020; (*b*) Z. Starosolski, R. Bhavane, K. B. Ghaghada, S. A. Vasudevan, A. Kaay and A. Annapragada, *PLoS One*, 2017, **12**, e0187563.

18 C. Maenz, E. Lenfert, K. Pantel, U. Schumacher, W. Deppert and F. Wegwitz, *BMC Cancer*, 2015, **15**, 178.

19 M. Poß, R. J. Tower, J. Napp, L. C. Appold, T. Lammers, F. Alves, C.-C. Glüer, S. Boretius and C. Feldmann, *Chem. Mater.*, 2017, **29**, 3547–3554.

20 Y. Yamamoto, I. Kawano and H. Iwase, *OncoTargets Ther.*, 2011, **4**, 123–136.

21 M. Poß, H. Gröger and C. Feldmann, *Chem. Commun.*, 2018, **54**, 1245–1248.

22 (*a*) S. Ehlers and U. E. Schaible, *Front. Immunol.*, 2013, **3**, 411–418; (*b*) C. Trefzer, M. Rengifo-Gonzalez, M. J. Hinner, P. Schneider, V. Makarov, S. T. Cole and K. Johnsson, *J. Am. Chem. Soc.*, 2010, **132**, 13663–13666.

23 S. Duchi, S. Ramos-Romero, B. Dozza, M. Guerra-Rebollo, L. Cattini, M. Ballestri, P. Dambruoso, A. Guerrini, G. Sotgiu, G. Varchi, E. Lucarelli and J. Blanco, *Nanomedicine*, 2016, **12**, 1885–1897.

24 (*a*) M. Yang, T. Yang and C. Mao, *Angew. Chem., Int. Ed.*, 2019, **58**, 14066–14080; (*b*) Z. Zhou, J. Song, L. Nie and X. Chen, *Chem. Soc. Rev.*, 2016, **45**, 6597–6626.